

Controlling the Frequency-Temperature Sensitivity of a Cryogenic Sapphire Maser Frequency Standard by Manipulating Fe^{3+} Spins in the Sapphire Lattice

K. Benmessai,¹ D.L. Creedon,¹ M. Mrad,² J.-M. Le Floch,¹ P.-Y. Bourgeois,² Y. Kersalé,² V. Giordano,² and M.E. Tobar¹

¹*ARC Centre of Excellence for Engineered Quantum Systems, School of Physics, University of Western Australia, 35 Stirling Hwy., Crawley 6009, Western Australia* ^{a)}

²*FEMTO-ST Institute, Time and Frequency Dept., 26 Rue de l'Épitaphe, 25 030 Besançon Cedex*

(Dated: 6 April 2018)

To create a stable signal from a cryogenic sapphire maser frequency standard, the frequency-temperature dependence of the supporting Whispering Gallery mode must be annulled. We report the ability to control this dependence by manipulating the paramagnetic susceptibility of Fe^{3+} ions in the sapphire lattice. We show that the maser signal depends on other Whispering Gallery modes tuned to the pump signal near 31 GHz, and the annulment point can be controlled to exist between 5 to 10 K depending on the Fe^{3+} ion concentration and the frequency of the pump. This level of control has not been achieved previously, and will allow improvements in the stability of such devices.

PACS numbers: 06.30.Ft, 07.57.Hm, 75.30.Hx, 76.30.-v

Keywords: Whispering Gallery Modes, Maser, Oscillator, Annulment temperature, Paramagnetic resonance, Fe^{3+}

^{a)}Electronic mail: karim.benmessai@uwa.edu.au

I. INTRODUCTION

The Whispering Gallery Mode Sapphire Maser is a stable microwave oscillator, which makes use of paramagnetic Fe^{3+} ions in ultra-low loss HEMEX cylindrical sapphire crystal at low temperature, and has been described in detail previously¹⁻⁵. The fractional frequency instability has been demonstrated to be as low as $\sigma_y(1s < \tau < 100s) = 10^{-14}$. This instability is normally measured at the frequency-temperature turnover point (or annulment temperature) of a high Q-factor ($> 10^9$) Whispering Gallery Mode (WGM) excited in the sapphire, where the effects of temperature fluctuations on frequency are nullified to first order by the magnetic susceptibility of residual paramagnetic impurities^{6,7}. Many publications describe the application of this self-compensation technique⁶⁻¹³, and all show that the annulment temperature is dependent on the presence and relative concentrations of paramagnetic ions such as Cr^{3+} with an Electron Spin Resonance (ESR) at 11.4 GHz, Mo^{3+} (100 GHz) and Ti^{3+} (1 THz). The ions are substitutionally included in the crystal lattice during the crystal growing process and occur unintentionally.

In this work we show that the frequency-temperature annulment for the Maser depends predominately on the Fe^{3+} ions and can be controlled by manipulating the number of ions involved in the maser process. We compare the behavior of two crystals - C1 (concentration of active Fe^{3+} ions = 10 ppb) and C2 (100 ppb). We also report the observation of an upper limit in temperature of 30 K for operation of the maser. This limit is explained using a Boltzmann distribution for the active ion, and we show that the populations of the energy levels are so close at this temperature that the effect of the pump at 31 GHz used to excite the maser at 12 GHz is negligible.

Controlling spins in such high-Q cavities could also have other potential applications. For example, it has recently been suggested that HEMEX sapphire with paramagnetic impurities could have applications for quantum measurement at millikelvin temperatures^{14,15}, such as qubits or quantum memory applications¹⁶⁻²².

II. MASER DESCRIPTION

The maser scheme is based on the three energy levels of Fe^{3+} ions at zero applied DC magnetic field in the sapphire lattice of a WGM resonator (Fig. 1). The concentration of

active ions used to create the effect is about 10-100 ppb, whereas the total concentration is on the order of 1 ppm. The bandwidth of the ESR is $\Delta\nu_{\text{Fe}^{3+}} \approx 27$ MHz, where the WG mode width is only $\Delta\nu_{\text{WG}} \approx 10$ Hz at 4.2 K.

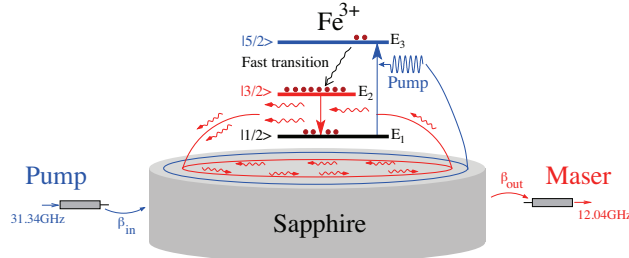


FIG. 1. *Principle of operation:* We apply a signal at 31.34 GHz, coinciding with a WG mode, to pump the ions from the lowest energy level $|1/2\rangle$ to the third $|5/2\rangle$. The ions then (non-radiatively) relax to the second energy level $|3/2\rangle$. A population inversion is obtained between the two lowest energy levels, and stimulated emission can be achieved at 12.04 GHz, which is enhanced by another WG mode coincident in frequency.

The maser signal frequency ν_{op} is fixed at the frequency ν_{WG} of the WG mode involved in the process. It is well known that the frequency ν_{WG} is strongly sensitive to temperature variations and needs to be precisely controlled. In this kind of resonator, ν_{WG} possesses a frequency-temperature turnover point (also referred as the annulment or annulment temperature) above 4.2 K, although annulment temperatures as low as 90 mK have been recently measured¹⁵. The frequency variations can be described by⁶:

$$\frac{\nu_{\text{WG}} - \nu_0}{\nu_0} = AT^4 + C(T, \nu) \quad (1)$$

where ν_0 is the mode frequency at 0 K without ions, and AT^4 is the thermal sensitivity due to the sapphire dilation ($A \approx 10^{-12}$ K⁻⁴ for our modes). The other term $C(T, \nu)$ is thermal sensitivity due to the paramagnetic ions and is defined by:

$$C(T, \nu) = \frac{1}{2} \sum_i \eta_i(\nu) \chi_0^{(i)} \frac{(2\pi\tau_2^{(i)})^2 \nu_i (\nu_i - \nu)}{1 + (2\pi\tau_2^{(i)})^2 (\nu_i - \nu)^2} \quad (2)$$

This term depends in reality on both temperature and operational frequency. The annulment temperature is then calculated by considering the maxima of Eqn. 2, where the index i labels the different paramagnetic species present in the lattice. The magnetic filling factor η_i of the

mode describes its magnetic field distribution in relation to the i^{th} species of paramagnetic ion, and $\chi_0^{(i)}$ is the DC magnetic susceptibility of that ion. As the operating frequency is fixed at around 12.04 GHz, only the effect of the Fe^{3+} is considered (i.e. the summation in Eq. 2 is only performed over a single ion $i = \text{Fe}^{3+}$), and the annulment temperature (T_{inv}) can then be expressed as follows^{6,23}:

$$T_{inv} = \left(\frac{(g\mu_B)^2 \mu_0 \pi \tau_2 \nu_{12} \sigma_{12}^2 N_{int}}{48k_B A} \right)^{\frac{1}{5}} \quad (3)$$

where the Bohr magneton $\mu_B = 9.274 \times 10^{-24} \text{ J.T}^{-1}$, the Boltzmann constant $k_B = 1.38 \times 10^{-23} \text{ J.K}^{-1}$, the Landé g-factor $g \approx 2$, $\sigma_{12}^2 \approx 2$ is a characteristic constant of the absorption rate of the ions at 12.04 GHz (calculated from the Fe^{3+} Sapphire spin Hamiltonian parameters)²³⁻²⁵, the spin-spin relaxation time τ_2 is related to the width at half resonance of the ESR ($\Delta\nu_{12} = 1/\pi\tau_2$). If two spins are in phase, and one absorbs a photon causing a phase shift, τ_2 is the necessary time for the spins to be in phase again.

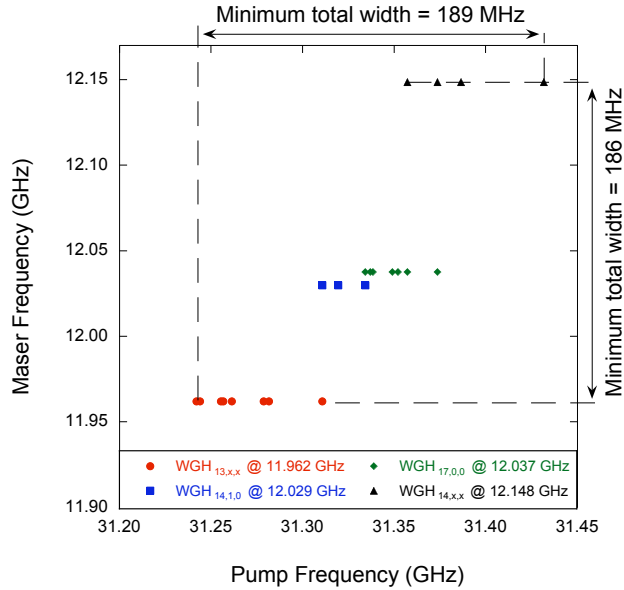


FIG. 2. The active maser bandwidth over which we can generate a signal is of order 180-190 MHz for crystal C2. Masing occurs at discrete frequencies where WGMs exist between 11.95 to 12.15 GHz, which are in turn pumped at discrete frequencies between 31.24 to 31.44 GHz where higher frequency WGM's exist.

Fig. 2 shows the bandwidth for active maser operation in crystal C2, which is more than 186 MHz for the 12 GHz and 31 GHz ESR levels. We can note from Fig. 2 that the maser

can operate in a multimode configuration. For example, when the pump frequency is in the range 31.350 GHz - 31.375 GHz, two signals can operate at once at 12.037 GHz and 12.149 GHz. In the rest of the paper, the characterization of the turnover temperature has been investigated for single-mode maser operation. We consider then in this paper $\Delta\nu_{12} = 27$ MHz, the width measured by Bogle and Symmons²⁶. N_{int} is the concentration of the active ions involved in the annulment temperature, in units of ion/m³. However, it is convenient to express it as a fraction of the Al₂O₃ in the crystal, i. e. 2.35×10^{22} ion/m³ \equiv 1 ppm. This concentration is related to the total ion concentration in the lattice as follow:

$$N_{int} = \zeta \times N_{total} \quad (4)$$

where ζ is the fraction of the ion concentration involved in the proces ($0 \leq \zeta \leq 1$) and N_{total} the total ion concentration in the lattice. When $\zeta = 0$, no frequency-temperature annulment is observed, and when $\zeta = 1$ all the ions in the lattice participate in the annulment process. Fig. 3 shows that the annulment temperature T_{inv} increases with the total number of ions

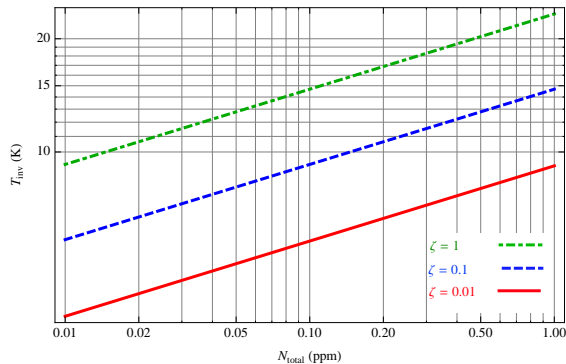


FIG. 3. Evolution of the annulment temperature with the total Fe^{3+} concentration for different values of the fraction ζ .

N_{total} .

III. MEASUREMENTS

To characterize the maser signal, we amplify it by 30 dB and then compare it to a signal from a synthesizer referenced to a hydrogen maser. The beat note is then amplified and band pass filtered before being counted (Fig. 4). The accuracy of the temperature control at the resonator cavity is about 2 mK.

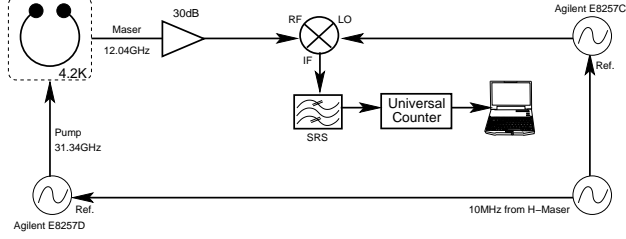


FIG. 4. *Experimental setup: The crystal is a cylindrical HEMEX sapphire, 30mm height and 50mm diameter, placed in a cylindrical cavity and cooled to 4.2 K using a cryocooler.*

A. Behavior of C1 with low concentration of Fe^{3+}

The maser characterized in this section oscillates at the $\text{WGH}_{17,0,0}$ mode frequency (12.038 GHz) of crystal C1, and can be excited using a pump signal corresponding to any of several WG modes around 31.34 GHz. The frequency of the WG mode that enhances the maser signal shows a turnover temperature T_{inv} around 7.8 K, with no dependence on the input power applied to the crystal. The evolution of the maser frequency with temperature is shown in Fig. 5.

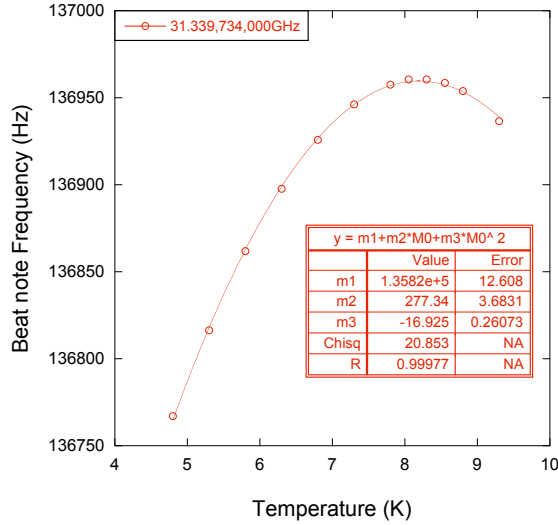


FIG. 5. *Evolution of the maser frequency (for C1) at 12.038 GHz with temperature for a fixed pump at 31.339,734 GHz. From the fit, the annulment temperature is 8.193 K.*

The excitation frequency of each pump WG mode was varied, and the evolution of the maser frequency with temperature was observed at various levels of pump power. The frequency was changed in steps of 250 Hz at various levels of pump power. As Fig. 6 shows,

T_{inv} is independent of the pump power and the pump frequency for each pump mode. For example, the 31.339 GHz pump mode has an annulment temperature which stays constant at 8.25 K.

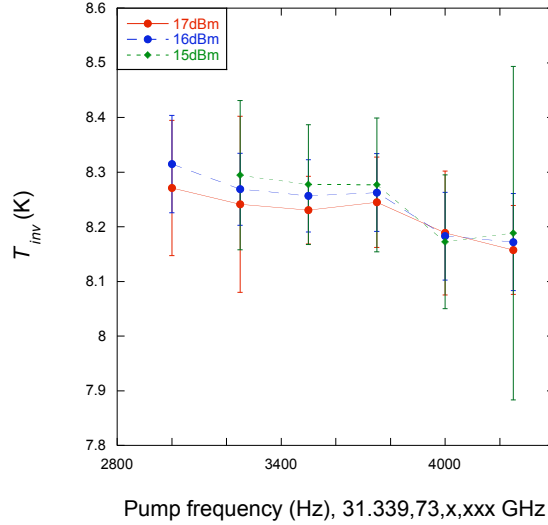


FIG. 6. Evolution of the annulment temperature for different values of the pump power and frequency. The pump mode chosen was at 31.339 GHz.

Despite the fact that T_{inv} is independent of the input power and frequency of the pump signal (for a particular choice of pump mode), its value does change when a different pump WG mode is selected, as shown in Fig. 7. The T_{inv} point is measured for the pump frequency range 31.320 - 31.339 GHz. No turnover point is observed at higher frequencies, due to the annulment temperature residing outside the measurable temperature range (below 4 K). T_{inv} can be calculated for each pump by a simple second order polynomial equation, as shown in Fig. 5.

For each pump at 31 GHz, the population of active ions N_{maser} used to create the maser signal is different from that fraction of ions that determine the T_{inv} for the mode. The active ion concentration was deduced for each T_{inv} from the maser output power calculated by Benmessai et al.²⁷, as shown by Eq. 5,

$$N_{maser} = \frac{1 + \beta_{out}}{\beta_{out}} \left[\frac{\beta_{out}}{Q_0} \frac{3k_B T \Delta\nu_{12}}{2\eta(g\mu_B)^2} \mu_0 \sigma_{12}^2 I_{ratio} \nu_{12} + \frac{2\tau_1}{3h\nu_{12}V_{eff}} \frac{2\Delta N_{23} + 5\Delta N_{13}}{\Delta N_{13}(\Delta N_{23} - \Delta N_{12})} \frac{Power}{\xi} \right] \quad (5)$$

The concentrations N_{maser} and N_{int} are the same only if the ESR is saturated. N_{maser}

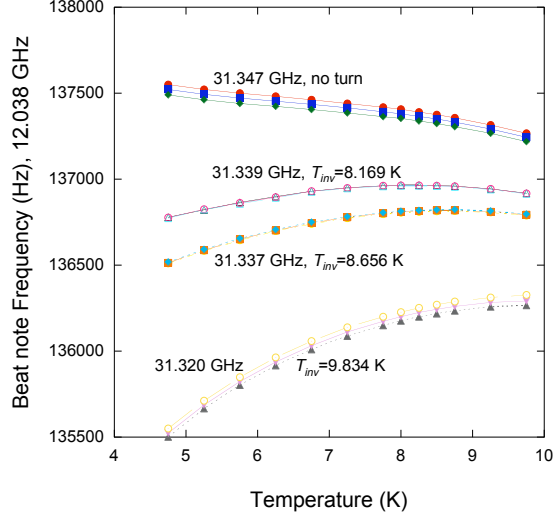


FIG. 7. Evolution of the maser signal frequency with temperature for different pumps at 31.3xx GHz. For each pump T_{inv} is independent from its frequency and the power.

is calculated from the rate equations and the Boltzmann law at saturation, and N_{int} is calculated from WG mode behaviour. The ion inversion ratio I_{ratio} is defined as follows:

$$I_{ratio} = \frac{(\Delta N_{23} - \Delta N_{12})(\Delta N_{13} + \Delta N_{23})}{\Delta N_{12}(5\Delta N_{13} + 2\Delta N_{23})} \quad (6)$$

where the different ΔN_{ij} are the normalized population difference between the energy levels i and j and are calculated as shown by Benmessai et al.²⁷. The relaxation time $\tau_1 \approx 10$ ms at 8 K is the spin-lattice relaxation time. This time is considered as constant around T_{inv} . In reality it undergoes a direct relaxation process and follows T^{-1} when $T \leq 15$ K^{28–30}. Here, β_{out} is the coupling of the mode at 12.04 GHz, Q_0 is its unloaded Q -factor, V_{eff} is the effective mode volume, η is the filling factor. The mode parameters are constant over the temperature range in which we characterize the signal, and are summarised in Table I.

TABLE I. Measured Parameters for the WGH_{17,0,0} mode at 8 K. The maser signal was operating on the lower doublet of the mode.

Mode	T_{inv} (K)	ν_{WG} (GHz)	β_{out}	$Q_0 \times 10^6$	V_{eff} (m^3)	η
WGH _{17,0,0}	7.8	12.038136	0.200	600	10^{-5}	0.99268
		12.038137	0.009	-		

By definition, ξ is the ratio between the power in the unsaturated regime and saturation ($0 < \xi \leq 1$). Note that for the pump at 31.337 GHz where the maser is at saturation, ξ should be equal to unity. From the results shown in Fig. 7, where T_{inv} is different from one pump to another, it is possible to calculate the corresponding concentration for each T_{inv} from Eq. (2). It is also possible to calculate the same concentration from Eq. (5). Knowing the maser output power, the result are shown in Table II.

TABLE II. Summary of the calculated concentrations

ν_{pump} (GHz)	T_{inv} (K)	Power (dBm) ^a	N_{int} (ppb) ^b	ζ	N_{maser} (ppb) ^c	ξ
31.320	9.834	-62.59	13.46	0.0135	7.74	0.6180
31.337	8.656	-60.50	7.11	0.0071	11.09	1.0000
31.339	8.169	-65.50	5.32	0.0053	3.57	0.3162
31.347	-	-69.00 ^d	-	-	1.90	0.1412

^a Measured at the output of resonator

^b Calculated from Eq. 3

^c Calculated from Eq. 5

^d at 9 K

Eq. (5) is evaluated when the maser signal is maximum (i.e. at saturation). As the maser signal is oscillating at one mode ($WGH_{17,0,0}$) for all the pumps, it is clear that for each pump the amount of active ions is different, leading to a calculation of different concentrations. Each pump has a different configuration of coupling and field distribution in the crystal. So, each pump will interact with a different quantity of ions, and whether saturation is reached is determined by the coupling.

B. Behavior of C2 with high concentration of Fe^{3+}

It has been shown previously⁵ that the concentration of Fe^{3+} ions in sapphire can be increased significantly by annealing in air, causing conversion of Fe^{2+} impurities to Fe^{3+} . Originally the two crystals C1 and C2 exhibited similar properties of very low concentration of Fe^{3+} impurities. However, C2 went through a series of additional annealing and was thus transformed from the low concentration regime (as reported here for C1) to the high concentration regime. The improvement in ion concentration is permanent, and once in the

high concentration regime the resonator will exhibit the effects reported in this paper. Thus, annealing a resonator is beneficial in two respects; due to the increased active ion population it will exhibit a higher maser output power, leading to a reduction in the Schawlow-Townes thermal noise limit⁴, as well as leading to a potential improvement in the curvature of the frequency-temperature dependence as is reported in this section.

For the crystal C2, the maser operation is very different as the concentration of the active ions is higher, resulting in a higher maser output power of -40 dBm, compared to -56 dBm for C1. In addition, maser signals are observed not only at the WGH_{17,0,0} frequency, but also at different modes whose frequencies are within the ESR bandwidth⁵. Like C1, all the pump modes for which a maser signal can be excited in C2 have a temperature turnover point independent of the applied power. Characterizing the turnover point for this crystal reveals more complex effects than C1.

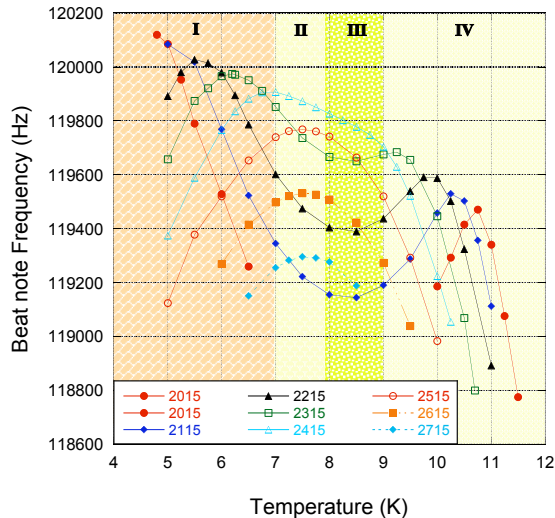


FIG. 8. Evolution of the maser signal frequency at 12.037 GHz with temperature for different value of the same pump at offsets (in Hz) from 31.349,780,000 GHz.

Figure 8 shows the signal at 12.037 GHz oscillating for a pump applied at 31.349 GHz. Each curve represents the maser frequency dependence as a function of temperature for different pump frequencies. Here, the maser frequency shows a strong dependence on the pump tuning. We note that when the frequency $\nu_{pump} \leq 31.349,782,315$ GHz, there are three T_{inv} – one near 6 K, the second around 8 K, and the third at 10.5 K. When $\nu_{pump} \geq 31.349,782,415$ GHz, there is only one T_{inv} around 8 K and the system behaves in the same classical fashion as the first crystal.

We can also divide the figure into four zones, with each zone defining a turnover temperature. From the results shown in Fig. 8, we can draw the evolution of the different turning point with the pump frequency (cf. Fig. 9).

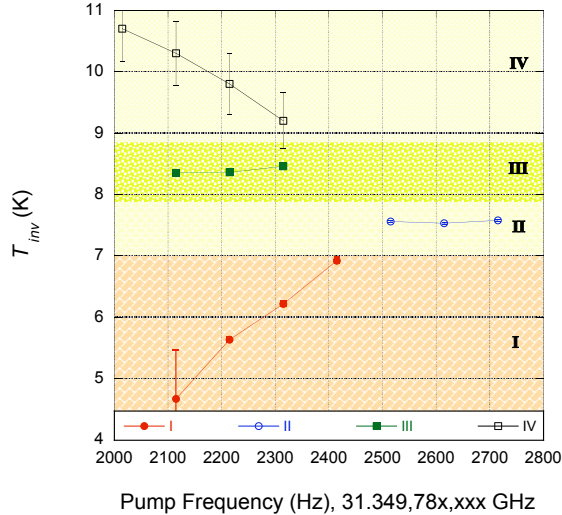


FIG. 9. Evolution of the turnover temperature at 12.037 GHz with different values of the same pump at offsets (in Hz) from 31.349,780,000 GHz.

The annulment exists for multiple temperatures only for the crystal C2 with high Fe^{3+} concentration. This effect appears to be nonlinear, showing that a variation in the active ion population is induced as the temperature is varied, which in turn changes the turning point temperature as the temperature is varied.

The annulment temperature depends on the distribution of the ions and the population difference between their levels. When the annulment temperature for the $\text{WGH}_{17,0,0}$ mode is measured using a network analyzer, no change is seen due to the small population difference at this frequency (5% of the total active population). However, when the maser is operating, i.e. being pumped, the configuration of the ions is completely different: population inversion exists between the $|1/2\rangle$ and $|3/2\rangle$ levels, and saturation is seen at 31 GHz where the population of the states $|1/2\rangle$ and $|5/2\rangle$ are equal. The population inversion rate is determined by the choice of pump mode near 31 GHz. For each pump mode, the strength of the maser signal depends on its coupling and spatial field distribution in the crystal. Strong coupling allows an optimum exchange of energy with the ions, and field distributions occupying more volume in the crystal increase the interactions with different classes of ions. Considering the inhomogeneous broadening of the line at 31 GHz in addition to these factors, we can

understand why T_{inv} is different from one pump to another. The Fe^{3+} spins act as individual packets selected by the pump WG mode corresponding. Thus, the pump signal selects a different quantity of ions among the broadened ESR frequency.

For C2, the case is more complex because T_{inv} is not only different from one pump to another for the same maser signal, but is different for the same pump mode when the frequency is tuned. The maser frequency shows more than one temperature turnover point for some pump frequencies, and no annulment for others. In the case where there is more than one, the curvature of annulment is significantly reduced, which has the potential to improve the stability and reduce the requirements of temperature control of the maser.

Optimum Operation

The characterization of the maser frequency with temperature was performed at a fixed pump frequency. However, the pump WG mode is temperature dependent as well as the WG modes near 12.04 GHz. To optimize the maser operation, it is necessary to tune the pump frequency for each operating temperature. This optimum frequency corresponds to maxima or minima of the maser frequency depending on the T_{inv} being measured. Fig. 10 shows how the maser frequency varies with temperature for different pump modes. The signal at

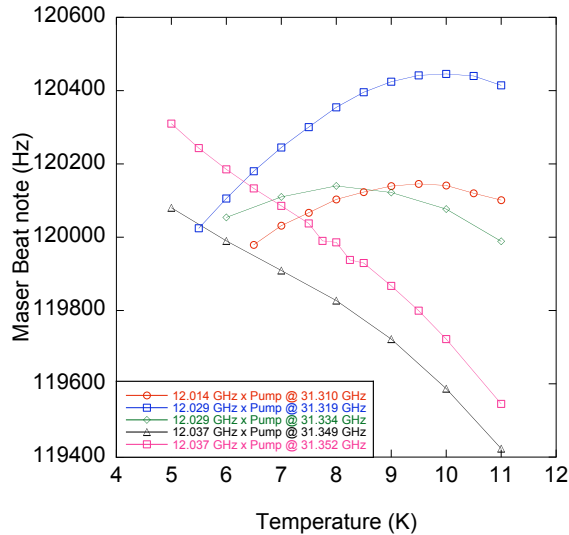


FIG. 10. *Evolution of the maser signal frequency with temperature for different pumps.*

12.014 GHz has a turnover point at 10 K, the one at 12.029 GHz is at 10.3 K, and the one

at 12.037 GHz shows no turnover temperature at all. The measurements were performed at different power levels, which were found to have no effect on the turnover temperature.

IV. MASER TEMPERATURE OPERATION LIMIT

In order to characterize the upper temperature limit $T_{operation}$ for maser operation, we adjust the pump frequency for each measurement as per the last section. The results are summarised in Table III. The 12.037 GHz maser signal oscillates until 28 K when pumped at 31.349 GHz, and 30 K when pumped at 31.352 GHz. The power of the maser signal is observed to decrease as the temperature is raised. This is due to the fact that the populations of the Fe^{3+} energy levels follow a Boltzmann distribution at thermal equilibrium. At higher temperatures, the difference in population between levels is reduced, resulting in less efficient masing. At high temperature (20-30 K) the number of ions pumped at 31.3 GHz is lower than at 4.2 K, leading to a smaller population inversion ratio. This directly affects the maser power and causes it to drop as temperature rises. In addition, the absorption at 31.3 GHz is a result of a mixing between the $|1/2\rangle$ and $|5/2\rangle$ spin states of the Fe^{3+} ion, which occurs with very small probability^{26,31,32}. The population difference at 31.3 GHz is high enough to excite the maser signal with this probability at low temperatures (<30 K), but not at high temperatures (>30 K). At higher temperatures still, characterization of the WG modes

TABLE III. Different annulment and operation limit temperatures for optimal operation of the maser

ν_{pump} (GHz)	ν_{maser} (GHz)	T_{inv} (K)	$T_{operation}$ (K)
31.310	12.014	9.407	15
31.319	12.029	9.910	26
31.334	12.029	8.140	23
31.349	12.037	-	28
31.352	12.037	-	30

around 12.04 GHz showed absorption effects up to 140 K. The strength of the absorption decreases when the temperature is increased, however no maser operation has been observed at these temperatures.

CONCLUSION

We have demonstrated how Fe^{3+} ions in a sapphire maser influence the frequency-temperature turnover point of the maser signal. We compared the behaviour of two crystals, one with a low active ion concentration and the other with a high concentration. The first crystal showed classical behaviour where T_{inv} is independent of the pump power and frequency, but was different between pump modes due to different packets of ions being excited for each pump. The population of ions that creates the maser causes a change in the intrinsic annulment temperature T_{inv} for the mode. The crystal with higher Fe^{3+} concentration showed a more complex behaviour, where T_{inv} was different not only from one pump mode to another, but showed many turnover points for some choices of pump, and in some cases none at all. Thus, the curvature of the annulment point in some cases could be reduced, which would also reduce the requirements for temperature control when generating a stable frequency.

ACKNOWLEDGMENTS

The authors wish to thank the Australian Research Council for supporting this work under grant numbers FL0992016, CE11E0082 and DP1092690, and ISL grant number FR100013.

REFERENCES

- ¹P.-Y. Bourgeois, N. Bazin, Y. Kersalé, V. Giordano, M. E. Tobar, and M. Oxborrow, “Maser oscillation in a whispering gallery mode microwave resonator,” *Applied Physics Letters* **87**, 224104 (2005).
- ²P.-Y. Bourgeois, M. Oxborrow, M. E. Tobar, N. Bazin, Y. Kersalé, and V. Giordano, “Maser oscillation from electronic spin resonance in a cryogenic sapphire frequency standard,” *International Journal of Modern Physics B* **20**, 1606 (2006).
- ³K. Benmessai, P.-Y. Bourgeois, Y. Kersalé, N. Bazin, M. E. Tobar, J. G. Hartnett, M. Oxborrow, and V. Giordano, “Frequency instability measurement system of cryogenic maser oscillator,” *Electronics Letters* **43**, 1436 (2005).

- ⁴K. Benmessai, D. L. Creedon, M. E. Tobar, P.-Y. Bourgeois, Y. Kersalé, and V. Giordano, “Measurement of the fundamental thermal noise limit in a cryogenic sapphire frequency standard using bimodal maser oscillations,” *Physical Review Letters* **100**, 233901 (2008).
- ⁵D. L. Creedon, K. Benmessai, M. E. Tobar, J. Hartnett, P.-Y. Bourgeois, Y. Kersalé, J.-M. LeFloch, and V. Giordano, “High power solid-state sapphire whispering gallery mode maser,” *IEEE Transactions on Ultrasonics, Ferroelectrics and Frequency Control* **57**, 282–285 (2009).
- ⁶R. P. Kovacich, A. G. Mann, and D. G. Blair, “Magnetic field tuning of paramagnetic frequency - temperature compensation in cryogenic sapphire dielectric microwave resonators,” *Journal of Physics D: Applied Physics* **30**, 3146–3152 (1997).
- ⁷A. G. Mann, A. J. Giles, D. G. Blair, and M. J. Buckingham, “Ultra-stable cryogenic sapphire dielectric resonators: mode frequency-temperature compensation by residual paramagnetic impurities,” *Journal of Physics D: Applied Physics* **25**, 1105–1109 (1991).
- ⁸J. G. Hartnett, M. E. Tobar, J.-M. LeFloch, J. Krupka, and P.-Y. Bourgeois, “Anisotropic paramagnetic susceptibility of crystalline ruby at cryogenic temperatures,” *Physical Review B* **75**, 024415 (1991).
- ⁹G. J. Dick, D. G. Santiago, and R. T. Wang, “Temperature-compensated sapphire resonator for ultra-stable oscillator capability at temperatures above 77K,” *IEEE Transactions on Ultrasonics, Ferroelectrics, and Frequency Control* **5**, 812–819 (1995).
- ¹⁰G. J. Dick, R. T. Wang, and R. L. Tjoelker, “Cryo-cooled sapphire oscillator with ultra-high stability,” in *Proceedings of the IEEE International Frequency Control Symposium and Exposition* (1998) pp. 528–533.
- ¹¹R. T. Wang and G. J. Dick, “Cryo-cooled sapphire oscillator with mechanical compensation,” *IEEE Transactions on Ultrasonics, Ferroelectrics, and Frequency Control* , 543–547 (2002).
- ¹²N. Boubekour, J. G. Hartnett, M. E. Tobar, N. Bazin, Y. Kersalé, and V. Giordano, “Frequency stability of Ti^{3+} -doped whispering gallery mode sapphire resonator oscillator at 34K,” *Electronics Letters* **9**, 534–535 (2005).
- ¹³M. E. Tobar, J. G. Hartnett, D. Cros, P. Blondy, J. Krupka, E. N. Ivanov, and P. Guillon, “Design of high-Q frequency-temperature compensated dielectric resonators,” *Electronics Letters*. **4**, 303–305 (1999).

- ¹⁴D. L. Creedon, M. E. Tobar, J. M. LeFloch, Y. Reshitnky, and T. Duty, “Single-crystal sapphire resonator at millikelvin temperatures: Observation of thermal bistability in high-Q factor whispering gallery modes,” *Physical Review B* **82**, 104305 (2010).
- ¹⁵D. L. Creedon, Y. Reshitnky, Y. Farr, W. Martinis, T. Duty, and M. E. Tobar, “High Q-factor sapphire whispering gallery mode microwave resonator at single photon energies and milli-kelvin temperatures,” *Applied Physics letters* **98**, 222903 (2011).
- ¹⁶T. Duty, “Towards superconductor-spin ensemble hybrid quantum systems,” *Physics* **3** (2010).
- ¹⁷F. Jelezko, T. Gaebel, I. Popa, A. Gruber, and J. Wrachtrup, “Observation of coherent oscillations in a single electron spin,” *Physical Review Letters* **92**, 076401 (2004).
- ¹⁸Y. Kubo, F. R. Ong, P. Bertet, D. Vion, V. Jacques, D. Zheng, A. Dréau, J.-F. Roch, A. Auffeves, F. Jelezko, J. Wrachtrup, M. F. Barthe, P. Bergonzo, and D. Esteve, “Strong coupling of a spin ensemble to a superconducting resonator,” *Physical Review Letters* **105**, 140502 (2010).
- ¹⁹D. I. Schuster, A. P. Sears, E. Ginossar, L. DiCarlo, L. Frunzio, J. J. L. Morton, H. Wu, G. A. D. Briggs, B. B. Buckley, D. D. Awschalom, and R. J. Schoelkopf, “High-cooperativity coupling of electron-spin ensembles to superconducting cavities,” *Physical Review Letters* **105**, 140501 (2010).
- ²⁰G. D. Fuchs, V. V. Dobrovitski, D. M. Toyli, F. J. Heremans, C. D. Weis, T. Schenkel, and D. D. Awschalom, “Excited-state spin coherence of a single nitrogen-vacancy centre in diamond,” *Nature Physics* **6**, 668–672 (2010).
- ²¹H. Wu, R. E. George, J. H. Wesenberg, K. Mølmer, D. I. Schuster, R. J. Schoelkopf, K. M. Itoh, A. Ardavan, J. J. L. Morton, and G. A. D. Briggs, “Storage of multiple coherent microwave excitations in an electron spin ensemble,” *Physical Review Letters* **105**, 140503 (2010).
- ²²I. Chiorescu, N. Groll, S. Bertaina, T. Mori, and S. Miyashita, “Magnetic strong coupling in a spin-photon system and transition to classical regime,” *Physical Review B* **82**, 024413 (2010).
- ²³K. Benmessai, *Maser Cryogénique à Modes de Gallerie*, Ph.D. thesis, Université de Franche-Comté (2008).
- ²⁴G. S. Bogle and H. F. Symmons, “Zero-field masers,” *Australian Journal of Physics* **12**, 1 (1958).

- ²⁵A. E. Siegman, *Microwave Solid State Masers* (Mc. Graw-Hill, 1964).
- ²⁶H. F. Symmons and G. S. Bogle, “On the exactness of the spin-Hamiltonian description of Fe^{3+} in sapphire,” *Proceedings of the Physical Society* **79**, 468–472 (1962).
- ²⁷K. Benmessai, P.-Y. Bourgeois, M. E. Tobar, N. Bazin, Y. Kersalé, and V. Giordano, “Amplification process in a high-Q cryogenic whispering gallery mode sapphire Fe^{3+} maser,” *Measurement Science and Technology* **21** (2010).
- ²⁸J. V. Vleck, “Paramagnetic relaxation times for titanium and chrome alum,” *Physical Review* **57**, 426–447 (1940).
- ²⁹R. Orbach and M. Blume, “Spin-lattice relaxation in multilevel spin systems,” *Physical Review Letters* **8**, 478–480 (1962).
- ³⁰J. Thorp and E. A. E. Ammar, “Spin-lattice relaxation in gadolinium-doped calcium tungstate,” *Journal of Materials Science* **11**, 1215–1219 (1976).
- ³¹L. S. Kornienko and A. M. Prokhorov, “Electronic paramagnetic resonance of the Fe^{3+} ion in corundum,” *Soviet Physics JETP* **13**, 1120–1125 (1961).
- ³²G. S. Bogle and H. F. Symmons, “Paramagnetic resonance of Fe^{3+} in sapphire at low temperatures,” *Proceedings of the Physical Society*. **73**, 531–532 (1959).